JOURNAL OF MECHANICAL ENGINEERING AND SCIENCES
ISSN: 2289-4659 e-ISSN: 2231-8380
VOLUME 20, ISSUE 1, 2026, 11108 - 11125
DOI: https://doi.org/10.15282/jmes.20.1.2026.7.0867

RESEARCH ARTICLE

Computational fluid dynamics analysis of wind-driven ventilation in a double-story terraced house sheltered by adjacent buildings

Bryan Phua Chu Yang[1], Muhammad Noor Afiq Witri Muhammad Yazid[1]*, Mohd Faizal Mohamad[2]

[1]Faculty of Mechanical Engineering, Universiti Teknologi Malaysia, 81310 UTM Johor Bahru, Johor, Malaysia
[2]School of Mechanical Engineering, College of Engineering, Universiti Teknologi MARA, 40450 Shah Alam, Selangor, Malaysia

Abstract - Natural ventilation (NV) is an effective method to enhance ventilation in enclosed areas or buildings without incurring any cost to fit in mechanical ventilation systems. In Malaysia, double- and triple-storey terraced houses account for a large share of residential properties. Hence, understanding the impact of NV on these types of houses is essential for achieving optimal air circulation and ensuring a healthy, comfortable living environment. The purpose of this study is to determine the optimal door-opening configuration for indoor ventilation in a typical Malaysian double-storey terraced house, under cross ventilation (CV) and single-sided ventilation (SSV), and to examine the influence of adjacent buildings. Computational fluid dynamics using OpenFOAM is used to evaluate ventilation on the house's ground floor under two prevailing wind directions: towards the front façade (forward wind) and towards the rear façade (backward wind). A validation study of a generic building block was conducted and compared against published experimental data. Our findings indicate that excluding upstream units leads to overestimations of approximately 100% to 150%, depending on indoor location. Additionally, CV configurations were significantly more effective than SSV configurations in terms of ventilation rate and area-weighted velocity. Under CV mode, wind enters the house through the opening at the back rather than the opening at the front, which faces the prevailing wind.

Article History
Received : 11 August 2025
Revised : 28 February 2026
Accepted : 16 March 2026
Published : 31 March 2026

Keywords
Natural ventilation
Cross ventilation
Single-sided ventilation
Double-storey terraced house
Computational fluid dynamics

1. Introduction

In modern times, more people live in urban areas than in rural areas. According to the United Nations [1], in 1950, only 30% of people lived in urban areas, but by 2014, this figure had skyrocketed to 54% and is expected to rise to 66% by 2050. In Malaysia, the urbanization rate increased to 75.1% in 2020, equivalent to 24.4 million people, up from 70.9% in 2010, or 19.5 million people [2]. The rapid urbanization in Malaysia has significantly shaped housing trends, particularly the prevalence of single- and multi-storey terraced houses within urban areas. Factors such as increased migration to urban centers for better economic opportunities, improved infrastructure, and access to amenities have contributed to the rising demand for housing in these areas. The residential building types in Malaysia include single- and multi-storey terraced houses, detached houses, townhouses, cluster houses, flats, condominiums, and apartments. According to the National Property Information Centre [3], there are a total of 1,419,736 two- and three-storey terraced houses in Malaysia in the first quarter of 2024, accounting for almost 22.8% of total residential properties and the highest category among property types. The affordability and space efficiency offered by double- and triple-storey terraced houses have made them a popular choice among urban residents seeking comfortable yet cost-effective dwellings.

In the context of these housing trends, building ventilation is essential for maintaining thermal comfort and indoor air quality. Building ventilation brings fresh outdoor air into a building while facilitating the circulation of indoor air. Unlike mechanical ventilation, natural ventilation (NV) relies on environmental forces such as wind pressure and buoyancy to drive airflow into the building [4]. A common NV strategy is cross ventilation (CV), which uses openings on opposite sides of a structure. This setup allows air to enter through an inlet on the windward side, move through the interior, and exit via an outlet on the leeward side. Typically wind-driven, CV relies on pressure differences between opposing wall openings [5]. In contrast, single-sided ventilation (SSV) involves all openings on a single building façade, regardless of their number or position. Unlike CV, SSV is not exclusively driven by wind; it can also be influenced by buoyancy or a combination of both mechanisms, particularly when openings are positioned at different heights [6]. Recent wind-tunnel results on wind-driven single-sided ventilation also show that façade flow separation near the opening can dictate the airflow direction through the opening and the resulting indoor circulation pattern [7]. Moreover, their analysis indicates that wind incidence angle has a statistically significant effect on ventilation rate and internal flow structure. Compared to SSV, CV usually delivers better airflow, more effective cooling, and improved indoor air quality. This is mainly because the pressure difference between the opposite walls in CV helps air move more efficiently through the space, reducing the chance of air recirculating or "short-circuiting" (a common drawback in SSV), and allowing indoor pollutants to be cleared more effectively [8, 9]. Nevertheless, recent computational fluid dynamics (CFD) results further confirm that cross-ventilation performance is highly sensitive to the opening configurations (inlet and outlet), the presence and dimensions of re-entrant spaces, and the distribution and orientation of windows [10, 11].

Several studies on natural ventilation have highlighted significant differences between unsheltered and sheltered buildings. Tominaga & Blocken [12] demonstrated that surrounding buildings reduce airflow rates by approximately

*CORRESPONDING AUTHOR | M.N.A.W. Muhammad Yazid | ✉ mnafiqwitri@utm.my
© 2026 The Author(s). Published by Universiti Malaysia Pahang Al-Sultan Abdullah Press. This is an open access article under the CC BY-NC 4.0 license

30%, altering velocity and concentration fields, and increasing concentration fluctuations in sheltered conditions. Using computational fluid dynamics, King et al. [13] compared airflow between a cube in isolation and in an irregular asymmetrical array at various prevailing wind angles. They found that ventilation rates for CV decrease by over 5% on average between the isolated case and the array configurations across all wind angles. The impact of wind direction has also been investigated by Zhang et al. [14] and Abdel Gelil Mohamed [15]. In another study, Golubić et al. [16] found that less densely spaced buildings achieve higher air change rates for CV, while SSV is more efficient in urban settings than in isolated settings. More recently, Miše et al. [17] showed that both atmospheric boundary-layer characteristics and building spacing can substantially alter ventilation intensity for isolated and sheltered buildings, and that cross-ventilation in closely packed neighborhoods is highly sensitive to wind incidence angle. Numerous studies have highlighted the importance of including more upstream and downstream structures [18-23]. These studies collectively emphasize the importance of accounting for surrounding buildings to represent dense urban layout accurately.

In Malaysia, terraced houses typically feature a car porch at the front of the house to shield vehicles from the elements (sun and rain) and a back alley at the rear of the house, which serves multiple purposes, such as sewerage conduits and emergency fire escape routes [24]. Moreover, the back alley is narrower compared to the main street at the front of the house. The house itself is characterized by its elongated layout, where the length often exceeds the width, which is a prevalent form of urban housing in Malaysia. The design reflects a practical use of space in densely populated urban areas, balancing vehicular access with outdoor living. However, the close proximity of neighboring properties and the layout of streets and buildings pose unique challenges to ventilation in these residential structures. Few studies have highlighted the importance of considering architectural elements such as ventilation openings, courtyards, shading, and mechanical devices to optimize ventilation and thermal comfort in terraced houses in Malaysia's hot and humid climate. Nugroho et al. [25] highlighted that single-sided ventilation in single-storey terraced houses in Malaysia often fails to provide adequate thermal comfort. Furthermore, the influence of overhang protrusions on the ventilation effectiveness of upwind and downwind buildings was numerically examined by Mohamad et al. [26]. The study revealed that the presence of overhang significantly modified the flow structure within the canyon and had a noticeable effect on the ventilation performance of the building located upwind. In another study, cross-ventilation was found to provide higher indoor air velocity than single-sided ventilation in a field experiment by Wellun et al. [27] in one room of a double-storey detached house. Using particle image velocimetry in a wind tunnel, Ali et al. [28] showed that the position of inlet openings significantly affects ventilation performance, with higher wind speeds observed in spaces with strategically placed openings. Tuck et al. [29] found that mixed-mode ventilation, combining natural ventilation with mechanical aids, offers better thermal comfort than free-running strategies alone. Other strategies to address indoor thermal comfort issues were demonstrated by Sadafi et al. [30] through the adoption of internal courtyards, which may improve thermal conditions through natural ventilation but may also increase temperatures in adjacent areas without proper shading. Toe and Kubota [31] explored vernacular passive cooling techniques that can be adapted to modern terraced houses. They emphasized the benefits of night ventilation, roof insulation, and small courtyards in maintaining indoor comfort.

According to the literature, terraced houses often provide inadequate ventilation, which can lead to deterioration of thermal comfort and intensify indoor air pollution, potentially compromising respiratory health and comfort among residents. Therefore, it is imperative to research terraced houses to understand better the quality of ventilation, which can affect residents' overall comfort and well-being. In addition, to the best of the authors' knowledge, most published studies have primarily focused on general ventilation strategies and have not adequately addressed the specific needs and performance of individual areas within a house. This knowledge gap is particularly evident in single-sided and cross-ventilation configurations, especially in terrace houses, where the impact on areas such as the living room, dining area, and kitchen remains underexplored. Moreover, many studies on natural ventilation in residential buildings have treated buildings as unsheltered and of generic shape, assuming unobstructed wind flow around the structure and open floor plans for interior layout. This assumption does not reflect the reality of many urban environments, where adjacent structures often shelter buildings, and interior partitions and/or layouts can be important. The presence of nearby buildings, combined with the segregated indoor layout, can significantly alter wind patterns and reduce the effectiveness of natural ventilation strategies. In light of the above matters, this study aims to determine how different door-opening configurations affect indoor ventilation in a double-story terraced house, with particular emphasis on the localized sheltering effect of the immediately adjacent units. The analysis focuses on natural ventilation, examining both cross and single-sided ventilation under two main wind directions: forward and backward. Rather than reproducing a fully developed urban canopy layer, the present study evaluates how the presence of nearby upstream and downstream structures alters outdoor–indoor airflow interaction in a typical residential layout.

2. Materials and Methods

2.1 Models and Computational Domain

Figure 1 shows a detailed schematic of a single unit of a double-storey terraced house located in the middle, which is the focus unit in this study, with the openings shown: front door (*F*), sliding door (*S*), and back door (*B*). The dimension (width × height) for the front door is 1 m × 2 m, the sliding door is 2 m × 2 m, and the kitchen door is 0.8 m × 2 m, corresponding to opening areas of 2 m^2, 4 m^2, and 1.6 m^2, respectively. The house unit has dimensions of 9.2 m × 5.7 m × 6.5 m (length × width × height). The unit is modelled according to Figure 2, which shows a photo of the terraced house located at Bukit Rahman Putra, Selangor, Malaysia. In this study, one row of houses is included upstream and downstream of the target house to account for the sheltering effect of the adjacent buildings. Compared to the end unit, the middle unit is expected to have much lower ventilation capacity due to the sheltering effect of the surrounding structures. The

minimum distance between the target house and the adjacent upstream units is 14 m, while the minimum distance to the downstream units is 2 m. The following describes the elements and modeling details of the target house. The ceiling height of the indoor unit is set to 2.5 m, and the wall thickness is set to 0.015 m. The model is further simplified by removing the top floor, since most social activities occur on the ground floor. The utility room and toilet on the ground floor are also excluded, as these rooms are typically closed. The staircase is also removed from the model, as the rooms upstairs are usually closed for privacy. The furniture, vegetation, vehicles, fence, occupants, and complex edges and eaves are not modelled, and the uneven spaces within the structures are levelled out, as this case study focuses only on how the layout of the empty terraced house affects indoor ventilation. With these simplification measures, the computational cost can be more efficient.

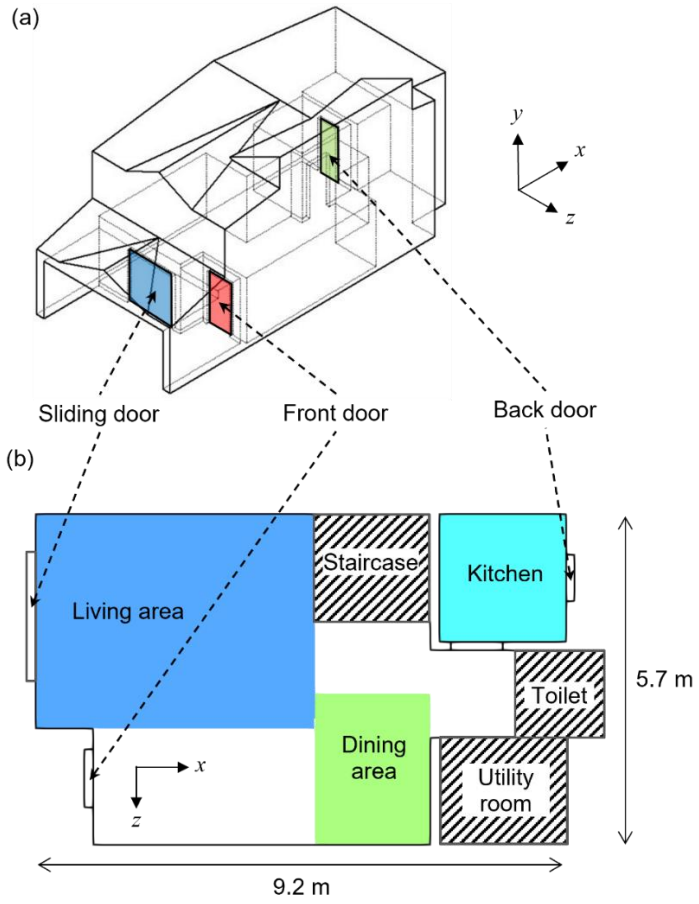

Figure 1. Detailed schematic of a single unit terrace house (a) opening and (b) space layout

Figure 2. Pictures of a single unit terrace house in (a) front view and (b) rear view

In this study, the impact of door openings is considered rather than that of window openings, as the door area is much larger than the window area, providing greater ventilation potential. In addition, two types of ventilation are compared: single-sided ventilation and cross ventilation. Table 1 presents the naming convention for all possible door-opening configurations considered in this study and will be used throughout the article. For example, the case "1FB" means the

ventilation type is cross ventilation with the prevailing wind in the windward direction onto the house's frontal façade, with the front and back doors opened, and the sliding door closed. The remaining configurations follow the same logic. In total, 14 cases are simulated, corresponding to different opening configurations and wind directions.

Table 1. Opening configurations considered in this study

Case	Ventilation type	Wind direction (1 or 0)	Front door	Sliding door	Back door
1F	SSV	Forward	Opened	Closed	Closed
1S	SSV	Forward	Closed	Opened	Closed
1B	SSV	Forward	Closed	Closed	Opened
1FS	SSV	Forward	Opened	Opened	Closed
1FB	CV	Forward	Opened	Closed	Opened
1SB	CV	Forward	Closed	Opened	Opened
1FSB	CV	Forward	Opened	Opened	Opened
0F	SSV	Backward	Opened	Closed	Closed
0S	SSV	Backward	Closed	Opened	Closed
0B	SSV	Backward	Closed	Closed	Opened
0FS	SSV	Backward	Opened	Opened	Closed
0FB	CV	Backward	Opened	Closed	Opened
0SB	CV	Backward	Closed	Opened	Opened
0FSB	CV	Backward	Opened	Opened	Opened

Three rows of houses were modelled following the recommendation of Yoshie et al. [32], with the target house in the middle row to include the shelter effect of the upstream and downstream row units. Here, only the center house on the street was modelled in detail, including its indoor and outdoor features, as it was the house of interest [33], whereas only the outer features of the surrounding houses were modelled to reduce computational cost significantly. The computational domain dimensions were defined as follows: an upstream length of 6*H*, a downstream length of 15*H*, and a height of 5*H* for both wind directions, as depicted in Figure 3, where the building model's height, 6.5 m, serves as the reference length (*H*). The lateral length of 2.75*H* was considered equivalent to three house units in the lateral direction. All the conditions stated in this section were applied to both the forward wind model and the backward wind model. The computational domain dimensions were selected in accordance with established urban wind CFD best practice guidelines. In particular, the upstream, downstream, and vertical extents were determined based on recommendations from the few guidelines [32, 33] to minimize blockage and ensure adequate wake development.

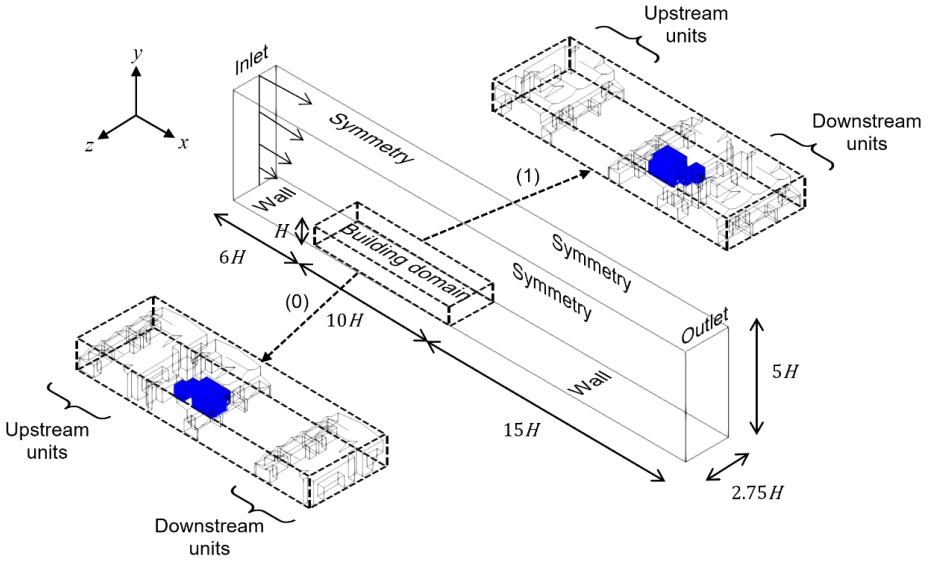

Figure 3. Computational domain size and boundary conditions. Inset: (1) and (0) label the building domain configuration under forward and backward wind direction, respectively. Blue colored body shows the indoor of the target house

In this study, the main road is wider than the back alley, which is expected to produce complex flow structures in these cavities. Depending on the building height-to-street width ratio, several flow structures may be observed [34, 35]. An avenue canyon ($H/W < 0.5$) is defined for the main road, characterized by isolated roughness flow. Conversely, a deep canyon ($H/W > 2$) is expected to form in the back alley of the target house, characterized by the formation of multiple

vertical vortices above the narrow street. Moreover, the study included an additional asymmetrical unit in the lateral direction, with symmetry applied at both ends.

2.2 Boundary Conditions and Solver Settings

A methodology for numerically simulating wind-driven ventilation was developed using the open-source CFD software OpenFOAM. The boundary conditions for the computational domain are indicated in Figure 3. For the inlet wind velocity profile, a logarithmic profile is used for the streamwise velocity component *U*:

$$U_h = \frac{u^*}{\kappa} \ln\left(\frac{h - h_0}{h_0}\right) \tag{1}$$

where h is the distance from the ground varying according to the *y*-axis, von Karman's constant κ of 0.41 is used, friction velocity, u^* is set to 0.2208 m/s, which is equivalent to 2 m/s at 10 m reference height and the aerodynamic roughness length, h_0 is set to 0.25 m. The chosen reference velocity is the typical value recorded by the weather stations at various sites in peninsular Malaysia [36], and the roughness length is chosen in accordance with the suburban landscape for terraced houses in Malaysia [37]. Symmetry boundary conditions are assumed at the lateral sides and top of the computational domain. It is worth noting that the periodic condition is not appropriate for the lateral sides in this study, given the asymmetrical structure of the house and the roof. In addition, zero static pressure is applied at the outlet, and the ground and building surfaces are assumed to be smooth.

In this study, the SST $k-\omega$ turbulence model is used to simulate turbulent flow, as it has been shown to provide reasonable accuracy in predicting cross ventilation [38, 39]. Although wind-driven ventilation is inherently unsteady, the present study focuses on time-averaged ventilation metrics. As will be discussed in Section 2.4, the steady-state Reynolds-Averaged Navier-Stokes (RANS) SST $k-\omega$ model demonstrates good agreement in predicting mean velocity distributions. Therefore, the steady approach is considered appropriate for evaluating average ventilation performance. It is acknowledged that transient simulations (e.g., large eddy simulation (LES) or unsteady RANS) may capture additional fluctuation-driven exchange processes beyond the scope of the current investigation. The variables of turbulent kinetic energy, k, and specific dissipation, ω, which are used as the inlet boundary conditions, are as follows:

$$k = \frac{3}{2}\left(U_{avg} I\right)^2 \tag{2}$$

$$\omega = C_\mu^{-1/4} \frac{\sqrt{k}}{l} \tag{3}$$

where U_{avg} is the average flow velocity, I is the turbulence intensity, which is given as 27.1% [40], l is the turbulent length scale, which corresponds to the indoor ceiling height of 2.5 mC_μ is the turbulence model constant, set to 0.09. At the outlet, all boundary conditions are set to zeroGradient, and the pressure is set to a constant zero value. The second-order method is used as the numerical scheme, and the Semi-implicit Method for Pressure-linked Equation algorithm is used for pressure velocity coupling. For the solver settings, the Generalized Geometric-Algebraic MultiGrid solver is used for the pressure, while smoothSolver is used for the other variables, with Gauss-Seidel as the smoother. For all simulations, the convergence criteria were set to 10^{-6} for pressure, velocity, and turbulent components.

2.3 Grid Settings and Grid Sensitivity Test

The computer-aided design models of the domain were generated using the open-source platform SALOME. The models were then discretized into unstructured tetrahedral meshes using the NetGen algorithm, which is integrated into SALOME. An unstructured tetrahedral mesh with prism layers was selected to accommodate the complex roof geometry, narrow street canyons, and interior openings. Mesh adequacy was verified through grid convergence analysis and validation. The maximum mesh size is 1.0 m, the minimum is 0.025 m, and the fineness is very fine. The local size setting for the house walls (outdoor and interior) and the vicinity of the terrace houses is set to 0.150 m. To accurately capture strong velocity gradients and jet development near openings, local refinement was applied around door boundaries and opening edges using the same refinement scale. Additionally, a viscous layer was applied to all wall and ground surfaces to resolve the boundary layer, with a minimum of 3 layers and a 1.2 stretch factor. The average wall y+ value over the target building surfaces was approximately 3.9, indicating that the first cell center lies within the viscous sublayer. This confirms that the near-wall region was adequately resolved for the SST $k-\omega$ turbulence model. With these settings, the generated mesh is approximately 3.9 million, herein labelled Mesh 2. The final mesh is shown in Figure 4. Mesh quality assessment showed a maximum non-orthogonality of 74.3 and a maximum skewness of 2.5 for this mesh. While the skewness has not exceeded the limit of 4, the non-orthogonality has exceeded 65 [41]. Thus, a non-orthogonal correction of 2 was applied to minimize discretization errors in regions of high non-orthogonality.

To verify the mesh's ability to resolve the flow, two additional simulations were carried out with coarse and fine meshes containing 1.5 million and 8.8 million cells, respectively. Herein, the 1.5 million-cell mesh is labelled Mesh 3, while the 8.8 million-cell mesh is labelled Mesh 1. In this study, one of the cross-ventilation cases (case 1FB) was used for the grid independence test. The grid convergence index (GCI) was calculated based on the streamwise velocity component (u) profiles at the center of the kitchen area (up to ceiling height), and at the center of the main road (up to the maximum computational domain height). The GCI is calculated as defined in Roache [42]:

$$GCI = F_s \frac{|u_{coarser} - u_{finer}|}{U_{ref}(r^p - 1)} \quad (4)$$

where F_s is the safety factor, set to 1.25 since three different numerical grids were used in the grid sensitivity test. The grid refinement factor, r is equal to $\sqrt{2}$, and the order of accuracy, p is set to 2, as all simulations employed second-order discretization schemes. The reference velocity, U_{ref} is the wind speed taken as 2 m/s at a height of 1.5H above the ground.

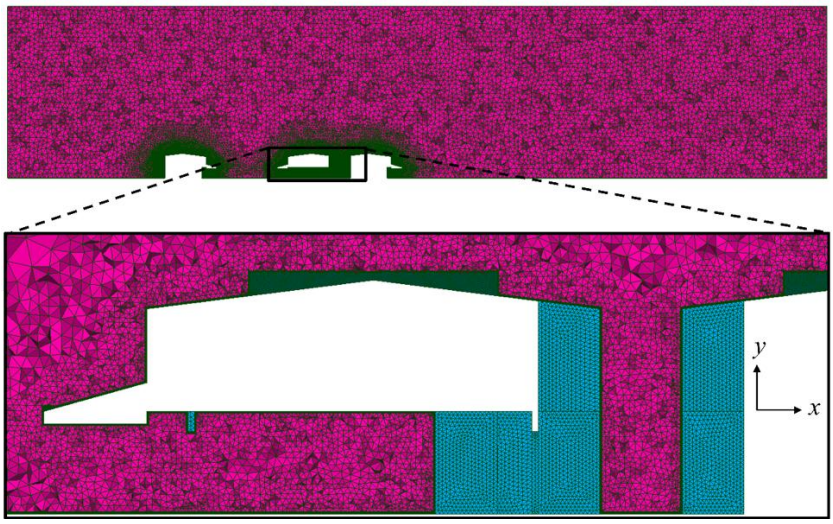

Figure 4. Unstructured tetrahedral mesh with a viscous layer for overall and in the vicinity of the target house unit

Figure 5 shows the velocity profiles at the center of the main road and kitchen area. In particular, the velocity profiles at the main road (in Figure 5(a)) show that the profile for the medium mesh is almost identical to the profile of the fine mesh. A closer examination of the inset of Figure 5(a) shows that the difference in velocity profile up to 5 m height between the coarse mesh and denser mesh is evident. In the kitchen, the medium mesh closely matched the fine mesh, except below 0.5 m in height. Although minor discrepancies were observed below 0.5 m height in the kitchen region, this area lies within the near-floor boundary layer where velocities are inherently small due to the no-slip condition. The ventilation performance metrics in this study were evaluated at 1.2 m above the floor (breathing level), which represents the occupied zone. Additionally, the relative differences in airflow patterns across mesh densities remained consistent. Therefore, the localized near-floor discrepancies do not affect the assessment of indoor airflow performance within the occupied zone. The calculated average $GCI_{3,2}$ and average $GCI_{2,1}$ at the center of the main road are 5% and 0.8%, respectively. Meanwhile, the calculated average $GCI_{3,2}$ and average $GCI_{2,1}$ at the center of the kitchen area are 4.5% and 1.7%, respectively. Thus, it can be said that the mesh resolution with 3.9 million cells used in this study is sufficient, as the average GCI between fine and medium meshes is well below 5% at both locations.

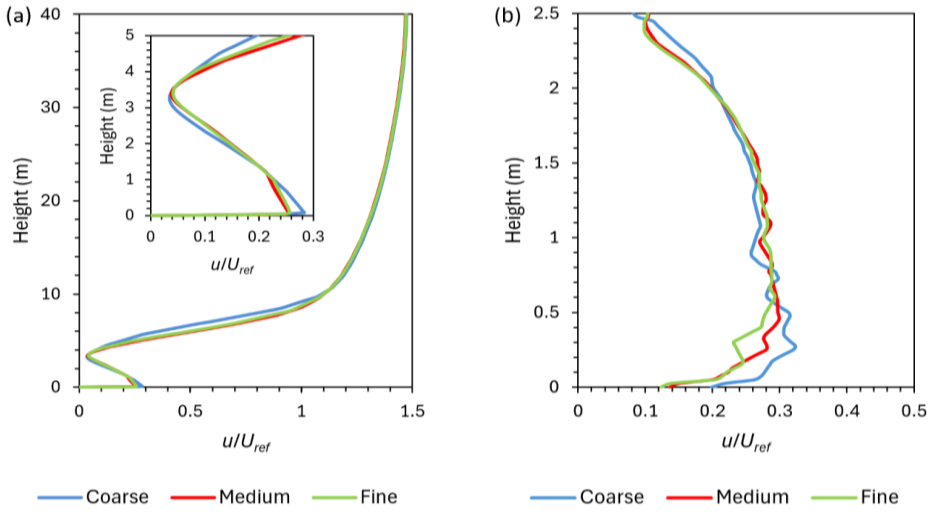

Figure 5. Vertical velocity profiles for grid independent test for case 1FB at the center of (a) main road, and (b) kitchen

2.4 Validation Test

The study is validated against Jiang et al. [43], which provides extensive experimental and large-eddy simulation results for flow inside and outside a cube-like model. Two ventilation cases have been considered for the validation: (1) CV with

openings on both windward and leeward sides, and (2) windward ventilation (WV) representing one type of SSV. The dimensions of the reduced-scale model are 250 mm × 250 mm × 250 mm (width × length × height). In both cases, the opening size is 84 mm × 125 mm (width × height), and the wall thickness is 6 mm. As in the case study, the computational domain size was modelled according to best-practice guidelines [32, 33]. The inlet boundary conditions for the validation test have been specified based on a RANS-based CFD study by Evola and Popov (2006) [44], which used a logarithmic profile for the streamwise velocity component. Prior to validation, grid independence was performed on the CV case using at least three meshes: about 400,000 cells, 800,000 cells, and 2,000,000 cells, corresponding to the coarse, medium, and fine meshes, respectively. In this study, the GCI between the fine and medium at *H*/4, *H*/2, and 3*H*/4 are 1.8%, 1.7%, and 2.4%, respectively. Thus, the medium mesh was used for comparison. Two validation metrics are used to verify the accuracy of the CFD setup of the present study, namely the Pearson correlation coefficient, R, and fractional bias (FB), defined as

$$R = \frac{\sum_{i=1}^{N}(P_i - \bar{P})(O_i - \bar{O})}{\sqrt{\sum_{i=1}^{N}(P_i - \bar{P})^2 \sum_{i=1}^{N}(O_i - \bar{O})^2}} \tag{5}$$

$$FB = \frac{\bar{O} - \bar{P}}{0.5(\bar{O} + \bar{P})} \tag{6}$$

where P and O are data from CFD simulations, and experiment works for sample i, N is the number of data points, and overbar symbols are the averaged values. The metric aims for 0 and 1 for FB and R, respectively. Here, an FB < 0.3 and R > 0.8 are considered good [45]. The simulation results using the SST $k-\omega$ model from this study were compared with the experimental data for both the FB and R for five velocity profiles inside and outside the building model under two ventilation modes (CV and WV), as shown in Table 2. In general, the SST $k-\omega$ model predicts the flow fields with good accuracy at -*H*/2, *H*/4, *H*/2, and 3*H*/4, indicated by the low FB (< 0.3) and small R (> 0.8). At *H* + *H*/2, however, the FB for WV is more than 0.4.

Table 2. Validation metrics for the velocity profiles at various positions in the streamwise direction under two ventilation modes

Ventilation type	CV		WV	
Index	FB	R	FB	R
Aim	0	1	0	1
-*H*/2	0.075	0.997	0.074	0.985
H/4	0.132	0.993	0.120	0.997
H/2	0.163	0.980	0.131	0.991
3*H*/4	0.198	0.962	0.213	0.960
H + *H*/2	0.226	0.824	0.419	0.924

Figures 6 and 7 compare the velocity profile, u/U_{roof} predicted by the SST $k-\omega$ model with that of the reference study, which is based on experimental data and large eddy simulation, at various streamwise positions for CV and WV, respectively. Here, the U_{roof} is 12 m/s at twice the height of the model (2*H*). Based on these velocity profiles, the present study provides a good prediction of the flow by capturing velocity variations near the model's height, similar to those captured by the LES in the reference study (see Figures 6(c-d) and 7(c-d)). However, the velocity above the model roof on the leeward side is predicted to be lower than in the reference study (see Figures 6(e) and 7(e)). The discrepancy between the results of this study and the reference study can be explained by the time-averaged velocity field used by the RANS-based model and the steady-state assumption in this study. The RANS-based model is renowned for its deficient estimation of momentum diffusion in the wake region behind buildings [46] and for its inherent limitations in accurately reproducing the transient fluctuations induced by vortex shedding around buildings [47]. Nevertheless, the present CFD method is considered acceptable, as the focus of this study is on the near-ground area for indoor and outdoor airflow, which the method captures. Hence, the outcomes of these validation tests confirm that the present CFD methods perform well in predicting indoor and outdoor flows at human height for both SSV and CV.

It is worth noting that the validation case involves a simplified cube geometry, whereas the present study considers a more complex terraced-house configuration. The cube benchmark primarily assesses the turbulence model's ability to predict bluff-body flow features, including separation, wake development, and mean velocity distributions. While this does not replicate the full geometric complexity of the terraced house, it provides confidence that the numerical framework captures the dominant aerodynamic mechanisms governing wind-driven ventilation.

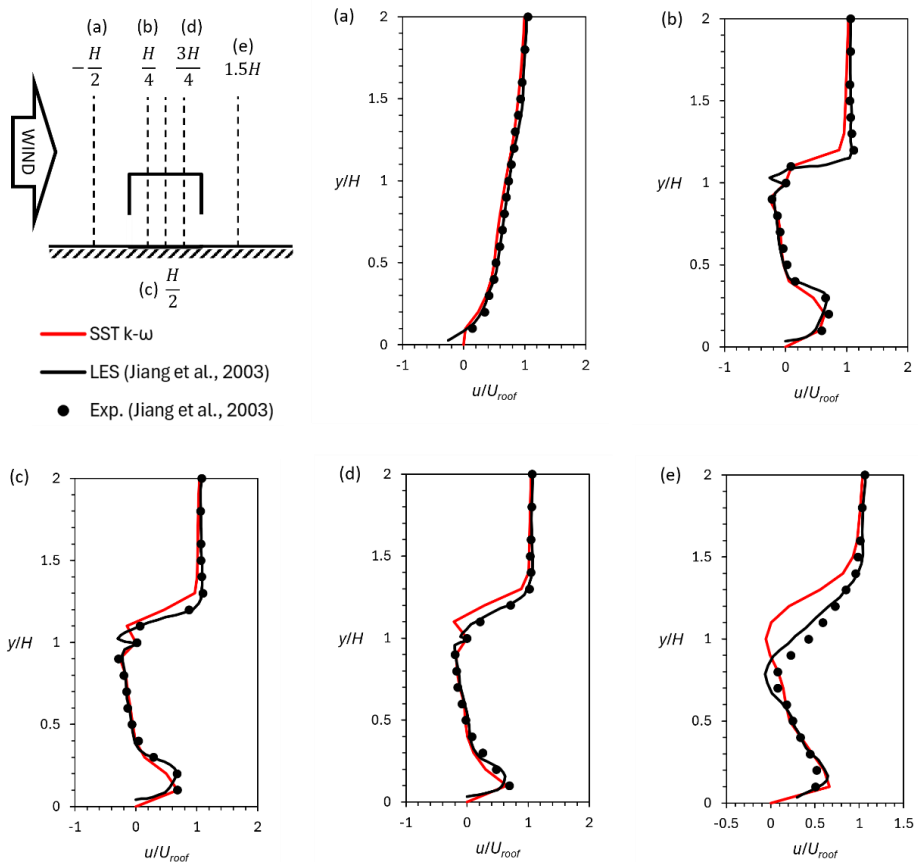

Figure 6. Vertical velocity profiles for validation of CV. Note: the black arrow indicates the inlet flow direction

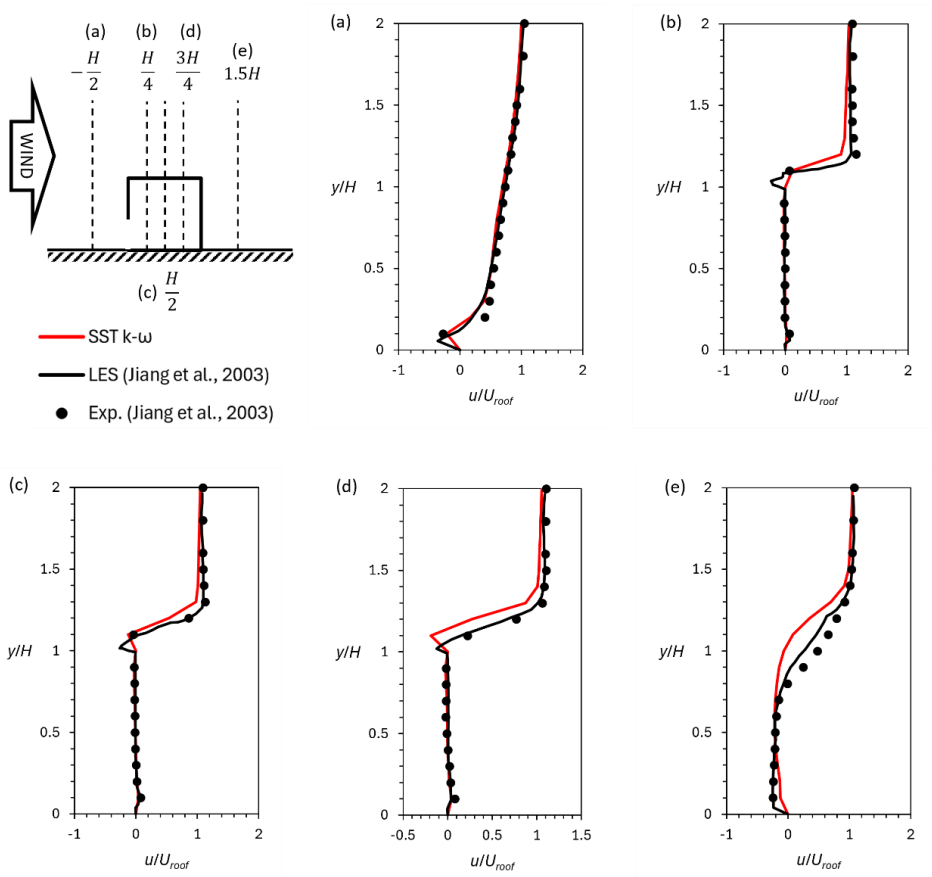

Figure 7. Vertical velocity profiles for validation of SSV. Note: the black arrow indicates the inlet flow direction

3. Results and Discussion

3.1 Flow Domain Sensitivity Analysis

A flow-domain sensitivity study was conducted without any adjacent units, with 1 row of upstream and downstream units, and using 1FB as the ventilation configuration. Additionally, a wider flow domain comprising five house units in the lateral direction was considered. Regardless of the building domain sizes, the same computational domain was used, as schematically shown in Figure 3. These cases were simulated to investigate the sheltering effects provided by the adjacent buildings. Figure 8 shows vertical velocity profiles for five domain cases at various indoor and outdoor spaces. For consistency, all results were extracted at the same locations as shown in the inset of Figure 8. A closer examination shows that none of the domain configurations involving upstream and/or downstream units exhibited a similar trend. In addition, the living area is generally less ventilated across all domain configurations, with velocities mostly below 5% of the reference velocity (see Figure 8(c)), whereas the kitchen area received higher velocities (see Figure 8(e)). Referring to Figure 8(a), the sheltering effect caused by the upstream unit is evident with the presence of a recirculation zone about the lateral axis, indicated by the gradual velocity reduction near the middle of the house height (about 3 to 4 m height from the ground). This effect extends into indoor space, where most areas exhibit velocities less than 30% of the reference velocity (see Figure 8(c-e)). On the other hand, the presence of upstream units generated higher velocities in the back alley of the target unit, particularly below 2 m in height, compared to cases without upstream units (see Figure 8(b)). This behavior can be explained by the different wake flow structures generated in both cases. In the case without upstream units, the air speed is generally low due to reduced flow recirculation in the back alley, as the recirculation zone is typically stronger in upstream units than in downstream units. Our findings demonstrate the importance of including the upstream units, as the model without upstream units has overpredicted the indoor velocity distribution at a few locations (at the center of the living, dining, and kitchen area) by nearly doubling the values of the case with upstream units (see Figure 8(c-e)).

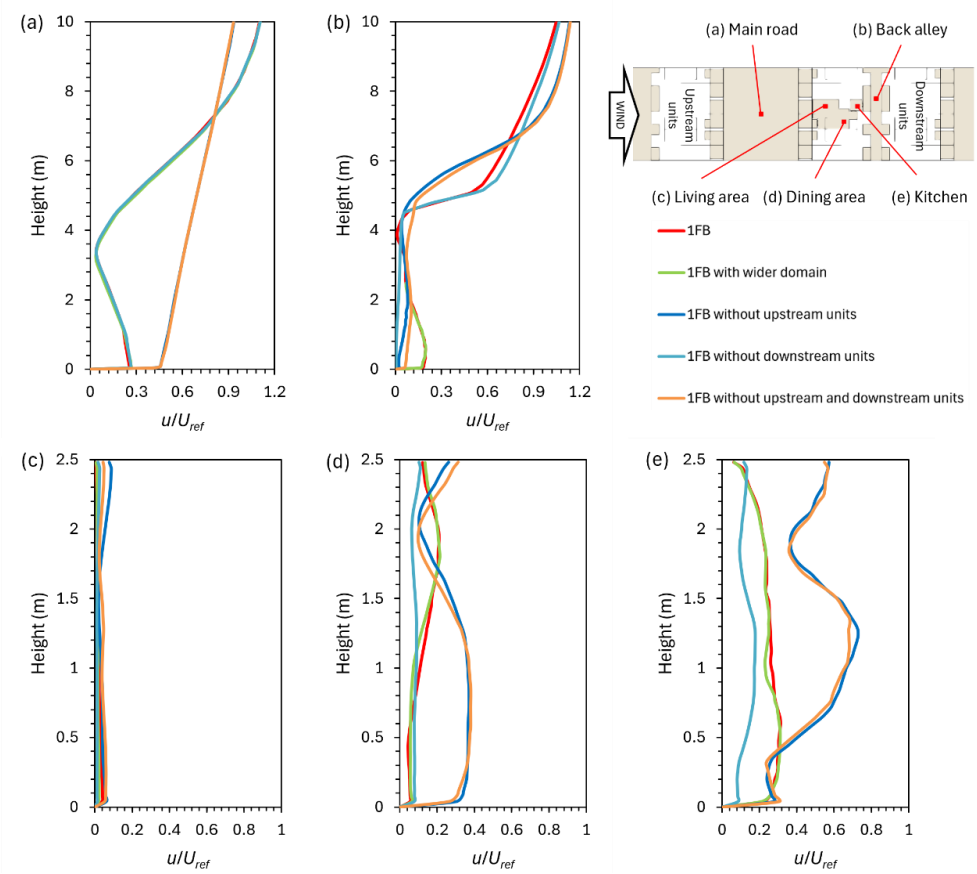

Figure 8. Vertical velocity profiles for different domain configurations at the center of (a) main road, (b) back alley, (c) living area, (d) dining area, and (e) kitchen area

In the domain without downstream units, specifically 1FB without downstream units, the velocity was observed to be the lowest, particularly in the back alley, dining area, and kitchen. A plausible explanation for this phenomenon is the formation of an isolated, relatively large recirculation behind the target building, as any adjacent units at the rear do not constrain it. However, another domain without downstream units, namely 1FB, which lacks both upstream and downstream units, does not exhibit the same trend. In this case, the overall velocity profiles are nearly identical to those in the 1FB case without upstream units across all examined locations. This similarity is due to the formation of separation flow over the roof corner of the target unit in both cases, resulting in an identical flow structure in the downstream region regardless of the presence of downstream units. Thus, the downstream unit does not play a significant role in the overall wind flow pattern when the upstream building is excluded from the model. Results indicate that increasing the domain

width has minimal impact on the vertical velocity profiles in both indoor and outdoor spaces. In some locations, the difference is less than 0.1 m/s on average. This suggests that it is sufficient to include at least one unit at both lateral ends of the target unit, even if the adjacent units are not physically symmetrical. Quantitatively, neglecting the upstream unit leads to a substantial overestimation of indoor ventilation, with peak indoor velocities overpredicted by approximately 100% in the dining area and up to 150% in the kitchen, compared to sheltered configurations, at heights less than 1.5 m. While previous studies have demonstrated that multiple upstream and downstream rows are required to reproduce a fully developed urban canopy layer [18-23], the present study focuses on the localized sheltering effect of immediate adjacent units. The subsequent section elaborates on the results and discussion for the scenario with one upstream, one downstream, and one lateral unit adjacent to the target unit.

3.2 Effects of Opening Configurations and Wind Directions

3.2.1 Ventilation rate

The results in Figure 9 highlight the significant impact of different opening configurations and wind directions on the net ventilation rate. Ventilation rate for each opening was calculated using an integral method [48, 49]. The so-called net ventilation rate, Q_{net} is mathematically defined as

$$Q_{net} = \sum_{i=1}^{N} u_{n,i} \cdot dA_i \tag{7}$$

where u_n is the normal velocity component, A is the area of the opening and the values are calculated at every numerical cell, i. The sign of the normal velocity was preserved during integration, such that inflow and outflow regions within the same opening were naturally accounted for. In cases where bidirectional flow occurred across the opening plane, the net ventilation rate represents the algebraic sum of inflow and outflow contributions. When multiple openings are present on the same façade, the net ventilation rate is obtained by summing the integrated flux across all openings.

For forward wind direction, the highest net ventilation rate is observed for the configuration with the sliding door and back door open (SB), at 0.57 m³/s (see Figure 9). The configurations with all doors open (FSB) also show high ventilation rates for both wind directions, with 0.48 m³/s for forward wind and 0.49 m³/s for backward wind. In contrast, the single-sided ventilation configurations (F, S, B) show significantly lower ventilation rates, with the front door (F) configuration having the lowest rate of 0.0035 m³/s. The front and sliding doors (FS) help improve ventilation by increasing the opening area, but the benefits do not outweigh the performance of the CV configuration. This indicates that SSV is less effective at promoting air circulation than CV setups, even with increased opening area. When the wind direction reverses, the net ventilation rates for all configurations increase slightly (see Figure 9). The SB configuration still maintains a high ventilation rate of 0.56 m³/s, while the SSV configurations show a noticeable improvement. For instance, the front door (F) configuration increases to 0.01 m³/s, and the sliding door (S) configuration increases to 0.02 m³/s. Hence, the backward wind direction might be more favorable for enhancing ventilation in SSV configurations, possibly due to the aerodynamic interactions with the building's structure. Further discussion of this trend will be provided in Section 3.2.3.

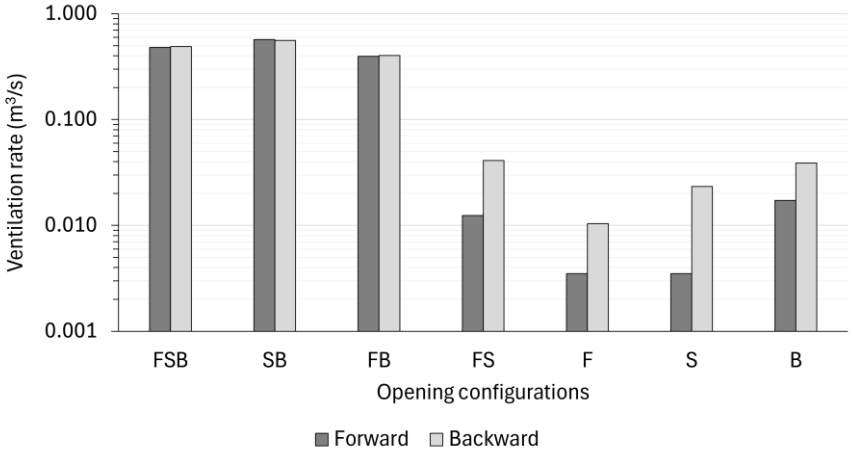

Figure 9. Net ventilation rate of various opening configurations and wind directions

3.2.2 Area-averaged velocity

Figures 10-11 provide insights into the area-averaged velocity at various indoor locations for different opening configurations and wind directions. The average velocity of a target area is calculated as the area-weighted average velocity magnitude, V defined as

$$V = \frac{\sum_i^N U_i \cdot dA_i}{\sum_i^N dA_i} \tag{8}$$

where U is the velocity magnitude. In this study, the data were extracted at a breathing level of 1.2 m above the floor level.

Figures 10(a) and 11(a) show that the dining area and the kitchen are generally the most well-ventilated areas of the house with CV configurations. For instance, under forward wind direction, all CV configurations achieve more than 0.1 m/s in the dining area and kitchen. These high velocities suggest that these areas benefit significantly from cross-ventilation setups, which create a strong airflow path through the house. The dining area, centrally located, lies along the airflow path between the front and back openings, ensuring consistent air movement. In contrast, the living area tends to be less ventilated than the dining area and kitchen, as the velocity is typically less than 0.1 m/s (see Figure 10(a)). This is because the air entering this space must spread out over a larger area.

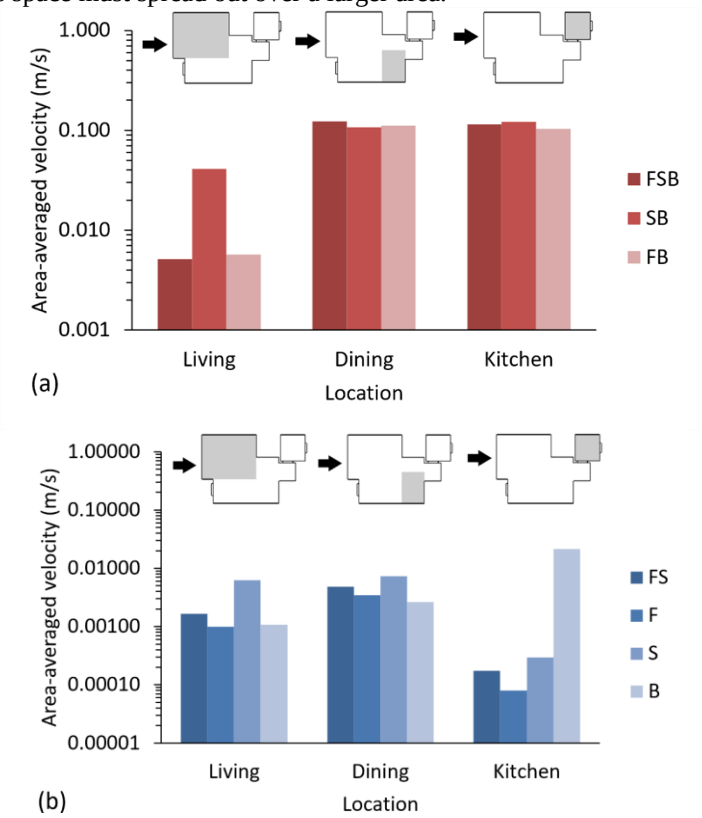

Figure 10. Area-averaged velocity at the living area, dining area, and kitchen area under forward prevailing wind for various opening configurations (a) CV and (b) SSV. Note: the black arrow indicates the inlet flow direction

On the other hand, Figures 10(b) and 11(b) show that the kitchen generally has lower average velocities than other areas of the house with SSV configurations. Here, the average velocity is a few orders of magnitude lower than in other areas. For example, with the front door open and wind blowing from the back, the area-average velocity in the living and dining areas exceeded 0.001 m/s, whereas the velocity in the kitchen was several orders of magnitude lower. On the contrary, the living and dining areas had higher velocities because they are located closer to the main openings, such as the sliding door and front door. This proximity allows these areas to benefit more directly from the airflow generated by these openings. In addition, the living and dining areas have fewer obstructions, which facilitates efficient ventilation. In comparison, the kitchen is located far from the front façade and is also enclosed, unlike other areas like the living or dining rooms, which can restrict airflow. It is important to note that the back-door-only configuration is the exception to this trend, in which the average velocities are a few times higher than in other SSV configurations, regardless of wind direction. Here, the kitchen is close to the back opening, so it is likely to experience better ventilation.

Comparing the ventilation rate and local area velocity, the higher net ventilation rates in Figure 9 generally correspond to higher local area velocities in Figures 10 and 11, particularly the CV configurations. For example, the SB configuration shows high net ventilation rates in Figure 9, which is reflected in the higher average velocities observed in the dining and kitchen areas in Figures 10-11. In contrast, the SSV configurations show lower local-area velocities, which are in line with the lower net ventilation rates. This indicates that an effective CV not only increases the overall air exchange rate but also enhances local air movement within specific areas of the house. However, the impact of wind direction on area-averaged velocity varies across different indoor areas. The living area consistently shows increased velocities exceeding 150% under backward wind for both CV and SSV, while the kitchen demonstrates substantial velocity increases under backward wind for CV, ranging from 52% to 137%. In contrast, the dining area under the backward wind for the FB case increases by approximately 16%, while the SB and FSB cases decrease by about 50%. These results indicate that wind direction effects are spatially non-uniform and depend strongly on opening configuration and airflow path alignment.

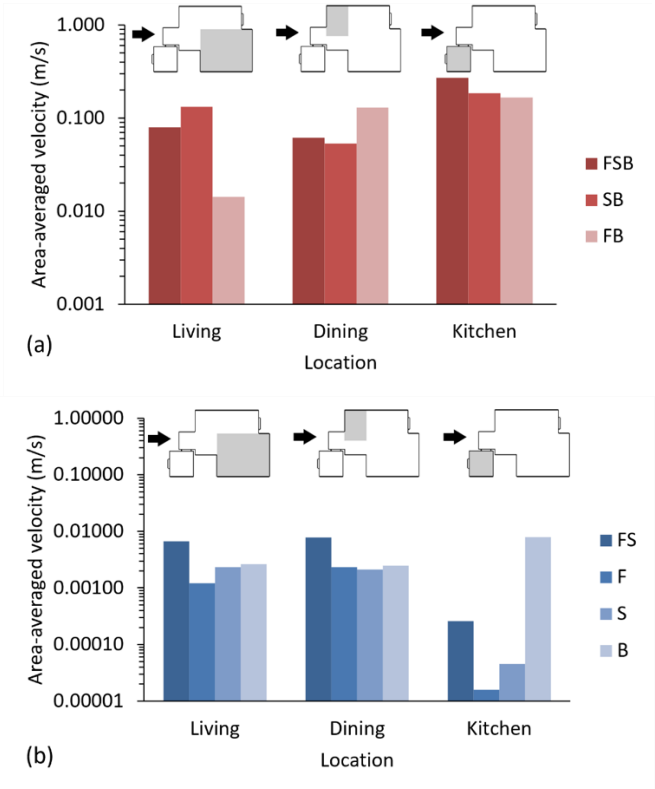

Figure 11. Area-averaged velocity at the living area, dining area, and kitchen area under backward prevailing wind for various opening configurations (a) CV and (b) SSV. Note: the black arrow indicates the inlet flow direction

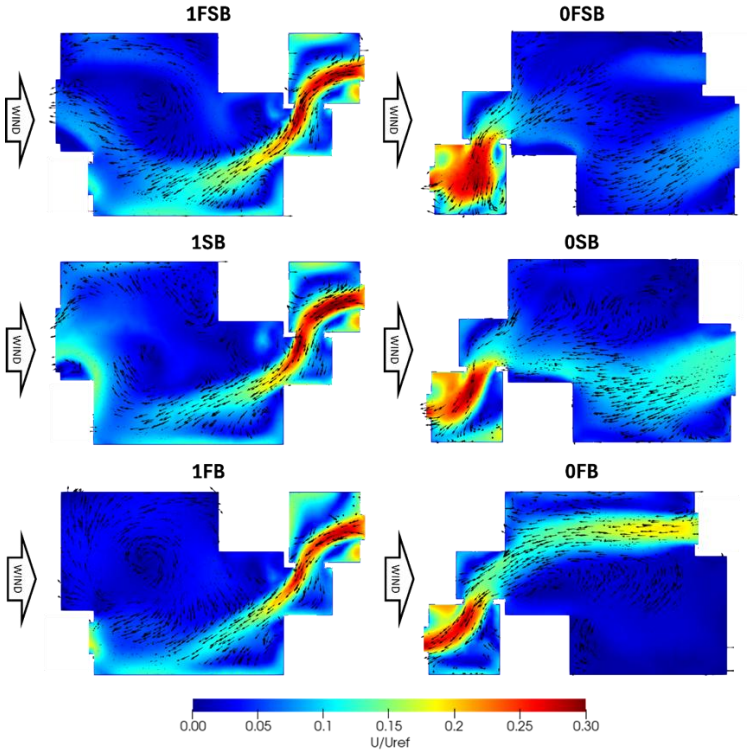

Figure 12. Normalized velocity magnitude and velocity vectors in the horizontal plane for CV configurations

3.2.3 Wind flow patterns

Figure 12 presents the normalized velocity magnitude, $U/U_{ref,}$ overlaid with velocity vectors in the horizontal plane at 1.2 meters above the floor for different CV configurations. The presence of recirculation zones is evident in all configurations, but their size and intensity vary significantly. Under forward wind, a vortex forms in the middle of the living area, while smaller eddies are formed in each corner of the house, creating very low speeds in this area. Meanwhile, most areas in the kitchen are well ventilated when subjected to CV, compared to the living area, due to its proximity to the back door

and its relatively small area. Effective flow across the openings, as clearly seen in 0SB (see Figure 12), is also attributable to the centralized location of the sliding door and the back door, which explains the high ventilation rate of the SB opening (see Figure 9). While 0SB exhibits only a localized low-speed region near one corner of the living area, 1SB shows a more pronounced recirculation zone due to the alignment of the dominant jet along the dining to kitchen axis. This observation highlights that a high overall ventilation rate does not necessarily eliminate localized stagnation zones, and that flow alignment relative to interior layout governs stagnant zone formation. The dining area, being in the middle, is located along the airflow path, allowing it to receive significant airflow. Despite being the least ventilated area, the living area can benefit when the sliding door is open, such as in 1FSB, 0FSB, 1SB, and 0SB. The 0FB configuration is particularly noteworthy for its consistently high flow along its path due to minimal resistance. However, this efficient flow pattern leads to very low wind speeds in the living area. Figure 12 also reveals how wind penetrates the house differently depending on the wind direction and configuration. For forward wind, the air enters primarily through the back door, while for backward wind, the flow enters through the front and/or sliding door.

Figure 13 presents the normalized velocity magnitude, u/U_{ref} overlaid with velocity vectors in the horizontal plane at 1.2 meters above the floor for different SSV configurations. Most areas in the house exhibit very low speeds except near the openings, with the door-only openings (1F and 0F) being the least effective. Additional openings (1FS and 0FS) do help improve the airflow in the interior, but the airflow still does not reach the kitchen effectively. Under SSV, the kitchen benefits the most from the opening of the back door. Remarkably, the back door opening under backwind conditions (0B) provides air ventilation deep into the house. It is important to note that the air speed in Figure 13 is significantly lower than in Figure 12, indicating superior ventilation performance of the CV compared to the SSV. Nevertheless, the occupants still benefit from the ventilation provided by the SSV, as indicated by the circulation throughout the entire interior space of the house.

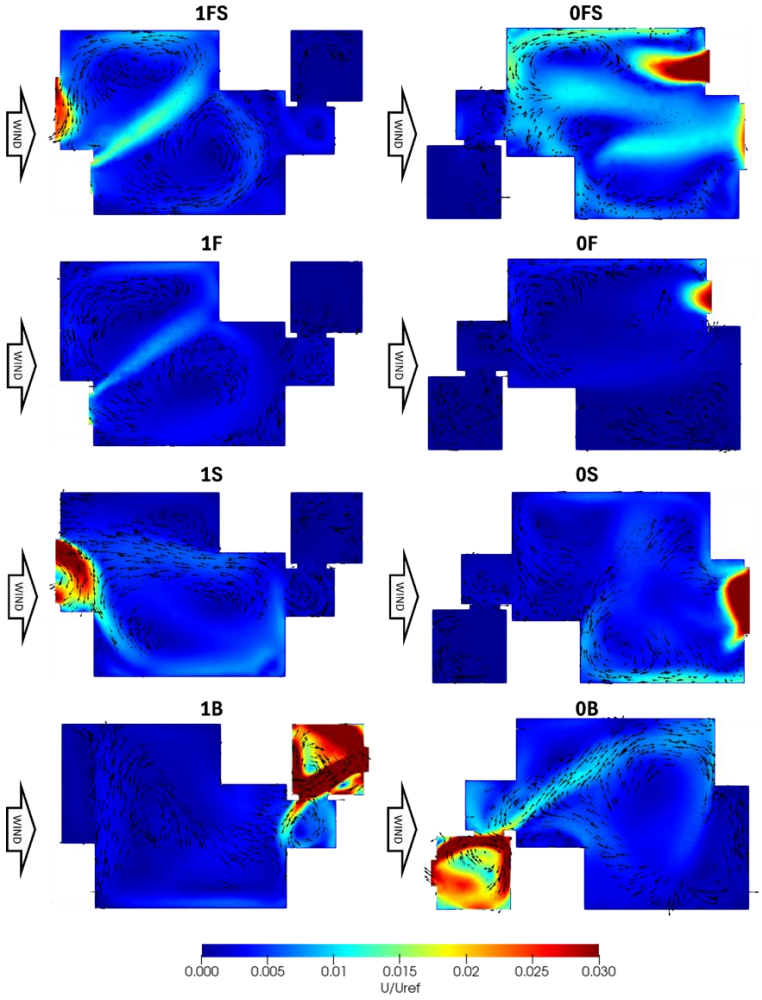

Figure 13. Normalized velocity magnitude and velocity vectors in the horizontal plane (at 1.2 m above the floor) for SSV configurations

Based on Figures 12-13, there is clear evidence that the wind flows indoors through the back of the house rather than through the front. To explain this peculiar flow behaviour, additional flow contours are extracted from a few cases. Figure 14 displays the pressure coefficient contour overlaid with a streamline in the vertical plane of the computational domain. The pressure coefficient is calculated as

$$C_p = \frac{p}{0.5\rho U_{ref}^2} \tag{9}$$

where p is the static pressure and ρ is the air density. Here, case 1FB and case 0FB are compared along with the cases without the adjacent buildings, labelled "without upstream and downstream units".

In the case of forward wind without adjacent buildings, flow separation is clearly visible in Figure 14(a), located near the roof corner of the target house unit. This separation is due to the sudden flow change caused by the building's sharp corners and creates a low-pressure region in the downstream area. The consistent pressure difference in the flow direction allows the air to enter the indoor unit from the windward side and exit through the leeward side, as there is no upstream obstruction. It is a different story for the case of adjacent buildings, as no clear flow separation is observed over the target house unit (see Figure 14(b)). Consequently, the pressure recovers in the downstream region of the target house unit, unlike in the upstream units, where the pressure is lower due to the separation flow at the upstream unit's roof corner. Therefore, there is an uneven pressure distribution in the subsequent streets, with lower pressure found in the street situated between the upstream and target house units. The same phenomenon observed in Figures 14(a-b) can also be seen in Figures 14(c-d) for the opposite wind direction. The uneven pressure regions could explain the peculiar flow behaviour observed in Figure 12 and 13, where the flow enters the indoor space through the back opening rather than the front. The results presented here show the significant impact of upstream buildings on the outdoor-indoor flow in the downstream region. To further elucidate the flow reversal mechanism, the pressure values at the front and rear openings were extracted and are shown in Figure 15. For the unsheltered case in 1FB, the front door exhibits positive pressure while the back door experiences suction, resulting in a pressure difference of approximately 1.82 Pa that drives airflow from front to rear. Conversely, in the sheltered case in 1FB, the front door experiences negative pressure, while the back door experiences even more negative pressure, yielding a reversed pressure difference of 0.20 Pa. This inversion of the façade pressure gradient explains the observed reversal of airflow direction and confirms that wake-induced pressure redistribution governs the indoor flow behavior.

Recapping the wind direction sensitivity observed for SSV in Section 3.2.1, it is primarily governed by opening pressure differences and momentum exchange driven by local shear layers, which manifest as a mean pressure distribution and near-opening recirculation. As shown in the pressure coefficient contours in Figure 14, the backward wind case produces a stronger low-pressure region and a larger pressure gradient along the rear alley than the forward wind case. Referring to Figure 15, the pressure difference for 1FB is about 0.2 Pa, while the 0FB is 0.24 Pa. This is consistent with the flow patterns in Figure 13, where a backward wind yields a stronger near-opening jet and greater recirculation than a forward wind. Although the results discussed here are based on one CV case, the trend has also been observed in SSV cases.

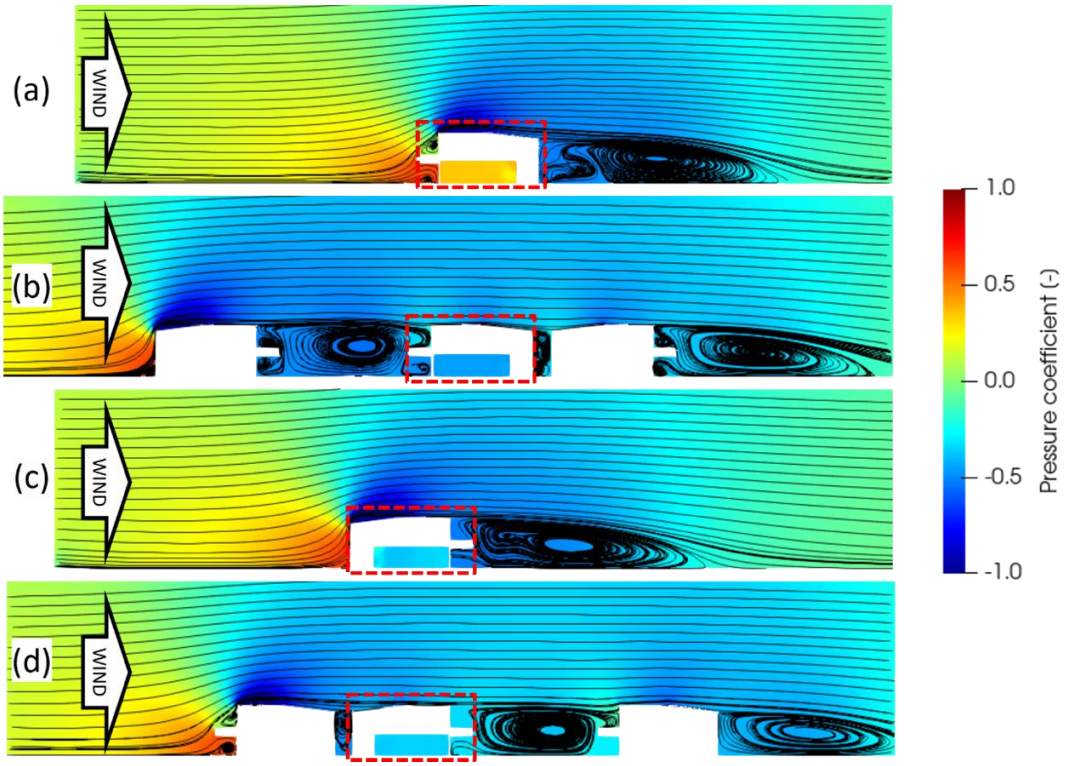

Figure 14. Pressure coefficient distribution of various street layouts and wind directions for (a) 1FB without upstream and downstream units, (b) 1FB, (c) 0FB without upstream and downstream units, and (d) 0FB

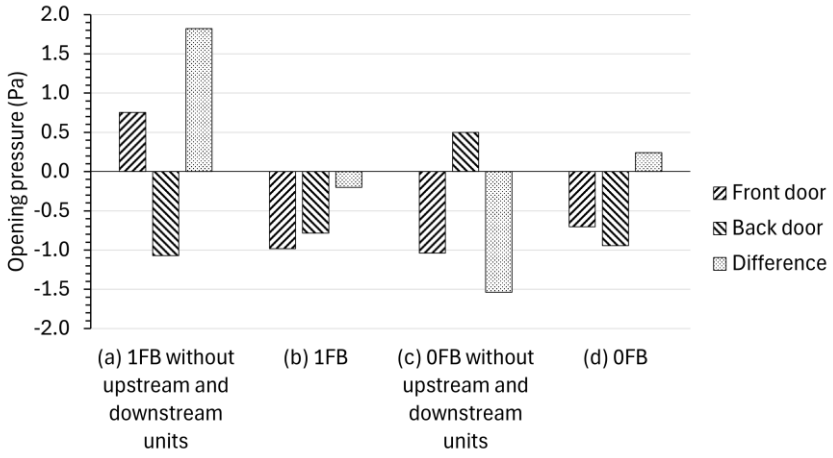

Figure 15. Opening pressure and pressure difference for the selected configuration

3.3 Model Limitations and Future Work

While the present findings demonstrate the significant sheltering influence of immediate upstream units for the investigated terraced-house configuration, future work may extend the computational domain to include multiple upstream and downstream rows to fully investigate the effects of a fully developed urban canopy and quantify the functional behavior of indoor ventilation performance under dense urban conditions. In addition, further studies may explore architectural modifications or alternative opening arrangements to mitigate localized stagnation zones identified in the present flow analysis, particularly in configurations where global ventilation performance does not guarantee uniform indoor airflow distribution. Besides, the quantitative magnitude of the upstream units' effect may also depend on building spacing, relative height, and façade porosity. Future work may conduct systematic parametric studies to assess the sensitivity of ventilation performance to these geometric variations and to extend the general applicability of the conclusions. It is noted that thermal comfort and indoor air quality compliance cannot be determined solely from airflow metrics, as they depend on additional factors such as temperature, humidity, occupant density, and contaminant generation. Future studies incorporating coupled thermal or pollutant transport modeling would be required for standards-based assessment.

4. Conclusions

Our findings show that including upstream units is crucial for creating the sheltering effect. The absence of these units led to overpredictions of indoor velocities, whereas downstream units had a lesser impact. Under the sheltering effect of adjacent buildings, cross-ventilation configurations generally outperformed single-sided configurations. The highest net ventilation rates, exceeding 0.5 m^3/s, were observed when both the sliding door and back door were open, particularly under forward wind conditions. Vector flow fields revealed that wind enters the unit through the back rather than through the front, relative to the prevailing wind. This flow reversal results from shelter-induced pressure redistribution caused by wake interaction from the upstream unit, which modifies the façade pressure field and alters the pressure gradient across the openings. As a consequence, airflow direction is governed by façade pressure differences rather than nominal wind direction. Additionally, backward wind conditions generally enhanced ventilation in cross-ventilation configurations, particularly in the living and kitchen areas, where area-averaged velocities increased by approximately 52% to 137% relative to forward wind. Area-averaged velocity analysis revealed that the dining and kitchen areas benefited most from the CV setups, achieving velocities exceeding 0.1 m/s, whereas the living area was less well ventilated. This observation indicates that high overall ventilation performance does not necessarily ensure uniform airflow distribution across all indoor zones. The comparatively lower ventilation in the living area is associated with a dominant airflow path that aligns preferentially with the primary openings, thereby limiting lateral momentum exchange. From a design perspective, this suggests that opening placement and internal layout configuration play a critical role in distributing airflow more evenly within terraced houses. In contrast, SSV configurations exhibited significantly lower ventilation rates and area-averaged velocities, with the kitchen being the least ventilated area, where the average velocity was a few orders of magnitude lower than in other areas. Although SSV provided the least ventilation, areas near the openings still experienced some airflow benefits. By strategically positioning openings, airflow can be enhanced. These findings offer valuable insights for improving natural ventilation strategies in double-storey terraced houses influenced by adjacent buildings.

Acknowledgements

The authors thank Universiti Teknologi Malaysia for providing the laboratory facilities that enabled this work.

Funding

This study was not supported by any grants from funding bodies in the public, private, or not-for-profit sectors.

Declaration of Competing Interest
The author declares no conflicts of interest.

CRediT Authorship Contribution Statement
Bryan Phua Chu Yang (Methodology; Investigation, Formal analysis; Visualisation; Writing - original draft)
Muhammad Noor Afiq Witri Muhammad Yazid (Conceptualization; Formal analysis; Supervision; Writing - review & editing)
Mohd Faizal Mohamad (Visualisation; Writing - review & editing)

Availability of Data and Materials
The data supporting this study's findings are available on request from the corresponding author.

Ethics Declarations
This study did not involve human participants or animals. Ethical approval was therefore not required.

Generative Artificial Intelligence Declarations
The authors stated that generative AI was not used to generate content, ideas, or theories. We have just utilised AI to enhance readability and refine the language. This was used with extreme human control and oversight. The authors take full responsibility for reviewing and approving the content.

References
[1] United Nations Department of Economic and Social Affairs, Population Division, *World Urbanization Prospects: The 2014 Revision*, (ST/ESA/SER.A/366), 2014.
[2] DOSM (Department of Statistics Malaysia), Key Findings of Population and Housing Census of Malaysia: Urban and rural, 2020.
[3] NAPIC (National Property Information Centre), Malaysia, *Residential Property Stock Table Q1 2024*, Valuation and Property Services Department, Ministry of Finance Malaysia, 2024.
[4] H. Y. Zhong, Y. Sun, J. Shang, F. P. Qian, F. Y. Zhao, H. Kikumoto et al., "Single-sided natural ventilation in buildings: A critical literature review," *Building and Environment*, vol. 212, p. 108797, 2022.
[5] U. Passe and F. Battaglia, Designing spaces for natural ventilation: An architect's guide, 1st ed. Routledge, 2015.
[6] C. Allocca, Q. Chen, and L. R. Glicksman, "Design analysis of single-sided natural ventilation," *Energy and Buildings*, vol. 35, no. 8, pp. 785–795, 2003.
[7] M. Stenech, G. Decitre, G. Brenn, and C. Irrenfried, "Experimental investigation of the ventilation efficiency for single-sided ventilation in suburban areas," *Building and Environment*, vol. 283, p. 113280, 2025.
[8] K. Niachou, S. Hassid, M. Santamouris, and I. Livada, "Experimental performance investigation of natural, mechanical and hybrid ventilation in urban environment," *Building and Environment*, vol. 43, no. 8, pp. 1373–1382, 2008.
[9] P. Karava, T. Stathopoulos, and A. K. Athienitis, "Airflow assessment in cross-ventilated buildings with operable façade elements," *Building and Environment*, vol. 46, no. 1, pp. 266–279, 2011.
[10] X. Fu, V. C. Tai, L. K. Moey, N. F. Abd Rahman, K. A. Ahmad, and D. Baglee, "Opening configurations and natural cross ventilation performance in a double-loaded multi-level apartment building: A CFD analysis," *Building and Environment*, vol. 254, p. 111404, 2024.
[11] P. Lin, H. Qin, S. S. Y. Lau, and Q. Wei, "Impact of unit type and configuration on indoor natural ventilation performance of high-rise, high-density residential buildings in Hong Kong," *Building and Environment*, vol. 269, p. 112444, 2025.
[12] Y. Tominaga and B. Blocken, "Wind tunnel experiments on cross-ventilation flow of a generic building with contaminant dispersion in unsheltered and sheltered conditions," *Building and Environment*, vol. 92, pp. 452–461, 2015.
[13] M. F. King, H. L. Gough, C. Halios, J. F. Barlow, A. Robertson, R. Hoxey et al., "Investigating the influence of neighbouring structures on natural ventilation potential of a full-scale cubical building using time-dependent CFD," *Journal of Wind Engineering and Industrial Aerodynamics*, vol. 169, pp. 265–279, 2017.
[14] X. Zhang, A. U. Weerasuriya, and K. T. Tse, "CFD simulation of natural ventilation of a generic building in various incident wind directions: Comparison of turbulence modelling, evaluation methods, and ventilation mechanisms," *Energy and Buildings*, vol. 229, p. 110516, 2020.
[15] N. Abdel Gelil Mohamed, "Assessment of urban ventilation in typical Egyptian housing layouts from four eras using a multi-directional CFD analysis," *HBRC Journal*, vol. 19, no. 1, pp. 453–481, 2023.
[16] D. Golubić, W. Meile, G. Brenn, and H. Kozmar, "Wind-tunnel analysis of natural ventilation in a generic building in sheltered and unsheltered conditions: Impact of Reynolds number and wind direction," *Journal of Wind Engineering and Industrial Aerodynamics*, vol. 207, p. 104388, 2020.
[17] D. Miše, C. Irrenfried, W. Meile, G. Brenn, and H. Kozmar, "Wind-driven natural ventilation of cubic buildings in rural and suburban areas," *Journal of Building Engineering*, vol. 87, p. 108740, 2024.

[18] M. J. Brown, R. E. Lawson, D. S. DeCroix, and R. L. Lee, "Mean flow and turbulence measurements around a 2-D array of buildings in a wind tunnel," in *Proceeding o 11th Joint AMS/AWMA Conference on the Applications of Air Pollution Meteorology*, Long Beach, CA, USA, 2000.
[19] Z. T. Ai and C. M. Mak, "CFD simulation of flow in a long street canyon under a perpendicular wind direction: Evaluation of three computational settings," *Building and Environment*, vol. 114, pp. 293–306, 2017.
[20] M. Llaguno-Munitxa, E. Bou-Zeid, and M. Hultmark, "The influence of building geometry on street canyon air flow: Validation of large eddy simulations against wind tunnel experiments," *Journal of Wind Engineering and Industrial Aerodynamics*, vol. 165, pp. 115–130, 2017.
[21] Z. Tong, Y. Chen, and A. Malkawi, "Defining the influence region in neighborhood-scale CFD simulations for natural ventilation design," *Applied Energy*, vol. 182, pp. 625–633, 2016.
[22] S. Liu, W. Pan, X. Zhao, H. Zhang, X. Cheng, Z. Long et al., "Influence of surrounding buildings on wind flow around a building predicted by CFD simulations," *Building and Environment*, vol. 140, pp. 1–10, 2018.
[23] S. Zheng, Y. Wang, Z. J. Zhai, Y. Xue, and L. Duanmu, "Characteristics of wind flow around a target building with different surrounding building layers predicted by CFD simulation," *Building and Environment*, vol. 201, p. 107962, 2021.
[24] N. M. Tawil, S. M. Lias, I. M. S. Usman, N. I. M. Yusoff, A. C. Ani, and K. A. Kosman, "Evolution of back lane design: A view of terrace housing in Malaysia," *Asian Social Science*, vol. 9, no. 15, p. 277, 2013.
[25] A. M. Nugroho, M. H. Ahmad, and D. R. Ossen, "A preliminary study of thermal comfort in Malaysia's single-storey terraced houses," *Journal of Asian Architecture and Building Engineering*, vol. 6, no. 1, pp. 175–182, 2007.
[26] M. F. Mohamad, A. Hagishima, J. Tanimoto, N. Ikegaya, and A. R. Omar, "On the effect of various design factors on wind-induced natural ventilation of residential buildings in Malaysia," in *Proceedings of 2nd Asia Conference of IBPSA-China, Japan, Korea*, 2014, pp. 139–146.
[27] Z. Wellun, W. F. M. Yusoff, M. F. Mohamed, M. K. A. M. Sulaiman, and M. R. M. Rasani, "Effects of single-sided and cross-ventilated sliding glass window openings on the indoor environment of a room in a hot and humid climate," *Jurnal Teknologi*, vol. 84, no. 6, pp. 107–114, 2022.
[28] N. M. Ali, M. F. Mohamad, W. Wang, C. Hirose, R. Yoshie, and N. Ikegaya, "Quantifying natural cross-ventilation flow of a two-layered model used for terraced houses in tropical zones by particle image velocimetry," *Building and Environment*, vol. 244, p. 110829, 2023.
[29] N. W. Tuck, S. A. Zaki, A. Hagishima, H. B. Rijal, M. A. Zakaria, and F. Yakub, "Effectiveness of free running passive cooling strategies for indoor thermal environments: Example from a two-storey corner terrace house in Malaysia," *Building and Environment*, vol. 160, p. 106214, 2019.
[30] N. Sadafi, E. Salleh, L. C. Haw, and Z. Jaafar, "Evaluating thermal effects of internal courtyard in a tropical terrace house by computational simulation," *Energy and Buildings*, vol. 43, no. 4, pp. 887–893, 2011.
[31] D. H. C. Toe and T. Kubota, "Comparative assessment of vernacular passive cooling techniques for improving indoor thermal comfort of modern terraced houses in hot–humid climate of Malaysia," *Solar Energy*, vol. 114, pp. 229–258, 2015.
[32] R. Yoshie, A. Mochida, Y. Tominaga, H. Kataoka, K. Harimoto, T. Nozu et al., "Cooperative project for CFD prediction of pedestrian wind environment in the Architectural Institute of Japan," *Journal of Wind Engineering and Industrial Aerodynamics*, vol. 95, no. 9, pp. 1551–1578, 2007.
[33] J. Franke, A. Hellsten, H. Schlünzen, and B. Carissimo, *Best Practice Guideline for the CFD Simulation of Flows in the Urban Environment*. COST European Cooperation in Science and Technology, 2007.
[34] T. R. Oke, "Street design and urban canopy layer climate," *Energy and Buildings*, vol. 11, no. 1-3, pp. 103–113, 1988.
[35] A. W. M. Yazid, N. A. C. Sidik, S. M. Salim, and K. M. Saqr, "A review on the flow structure and pollutant dispersion in urban street canyons for urban planning strategies," *Simulation*, vol. 90, no. 8, pp. 892–916, 2014.
[36] M. H. Hanipah, N. A. C. Sidik, R. Yunus, M. N. A. Yasin, and M. N. A. W. M. Yazid, "Assessment of outdoor thermal comfort and wind characteristics at three different locations in Peninsular Malaysia," in *MATEC Web of Conferences*, 2016, vol. 47, p. 04005.
[37] J. Wieringa, "Updating the Davenport roughness classification," *Journal of Wind Engineering and Industrial Aerodynamics*, vol. 41, no. 1-3, pp. 357–368, 1992.
[38] J. I. Perén, T. Van Hooff, B. C. C. Leite, and B. Blocken, "CFD simulation of wind-driven upward cross ventilation and its enhancement in long buildings: Impact of single-span versus double-span leeward sawtooth roof and opening ratio," *Building and Environment*, vol. 96, pp. 142–156, 2016.
[39] X. Qiu, J. Zhou, X. Xiao, W. Zhu, J. Zhang, S. Gui et al., "The numerical simulation study of pumping airflow driven by wind pressure for single-and multi-room buildings," *Buildings*, vol. 13, no. 12, Art. no. 3066, 2023.
[40] J. E. Cermak, *Wind Tunnel Studies of Buildings and Structures*. Reston, VA, USA: American Society of Civil Engineers, 1999.
[41] C. J. Greenshields, *OpenFOAM v13 User Guide*. The OpenFOAM Foundation, 2025.
[42] P. J. Roache, "Quantification of uncertainty in computational fluid dynamics," *Annual Review of Fluid Mechanics*, vol. 29, no. 1, pp. 123–160, 1997.

[43] Y. Jiang, D. Alexander, H. Jenkins, R. Arthur, and Q. Chen, "Natural ventilation in buildings: Measurement in a wind tunnel and numerical simulation with large-eddy simulation," *Journal of Wind Engineering and Industrial Aerodynamics*, vol. 91, no. 3, pp. 331–353, 2003.
[44] G. Evola and V. Popov, "Computational analysis of wind-driven natural ventilation in buildings," *Energy and Buildings*, vol. 38, no. 5, pp. 491–501, 2006.
[45] I. Goricsán, M. Balczó, M. Balogh, K. Czáder, A. Rákai, and C. Tonkó, "Simulation of flow in an idealised city using various CFD codes," *International Journal of Environment and Pollution*, vol. 44, no. 1-4, pp. 359–367, 2011.
[46] Y. Tominaga, S. Akabayashi, T. Kitahara, and Y. Arinami, "Air flow around isolated gable-roof buildings with different roof pitches: Wind tunnel experiments and CFD simulations," *Building and Environment*, vol. 84, pp. 204–213, 2015.
[47] M. Shirzadi, Y. Tominaga, and P. A. Mirzaei, "Experimental and steady-RANS CFD modelling of cross-ventilation in moderately-dense urban areas," *Sustainable Cities and Society*, vol. 52, p. 101849, 2020.
[48] Y. Adachi, N. Ikegaya, H. Satonaka, and A. Hagishima, "Numerical simulation for cross-ventilation flow of generic block sheltered by urban-like block array," *Building and Environment*, vol. 185, p. 107174, 2020.
[49] W. H. W. Ismail, M. F. Mohamad, N. Ikegaya, J. Chung, C. Hirose, A. Abd Razak et al., "Comprehensive comparisons of RANS, LES, and experiments over cross-ventilated building under sheltered conditions," *Building and Environment*, vol. 254, p. 111402, 2024.